Evidence for widely-separated binary asteroids recorded by craters on Mars

Dmitrii E. Vavilov, Benoit Carry, Anthony Lagain, Anthony Guimpier, Susan J. Conway, Hadrien Devillepoix, Sylvain Bouley

Graphical Abstract

Evidence for widely-separated binary asteroids recorded by craters on Mars

Dmitrii E. Vavilov,Benoit Carry,Anthony Lagain,Anthony Guimpier,Susan Conway,Hadrien Devillepoix,Sylvain Bouley

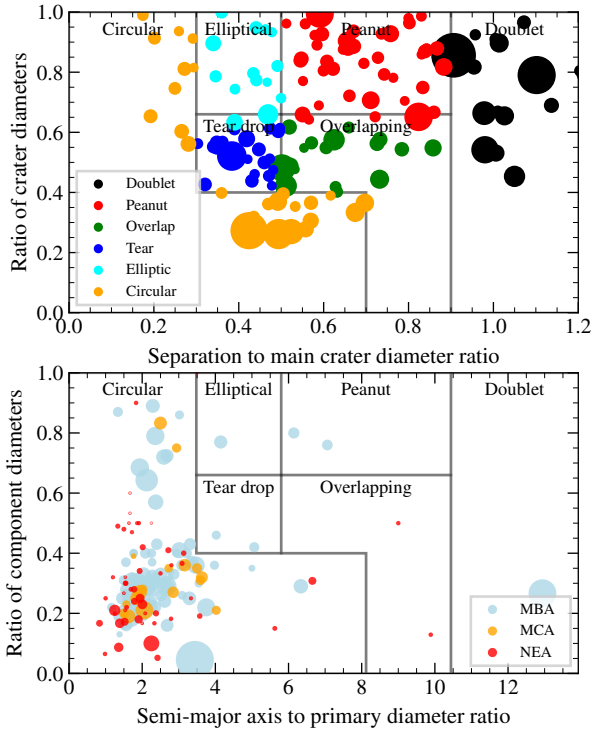

Highlights

Evidence for widely-separated binary asteroids recorded by craters on Mars

Dmitrii E. Vavilov,Benoit Carry,Anthony Lagain,Anthony Guimpier,Susan Conway,Hadrien Devillepoix,Sylvain Bouley

- First database of Martian binary craters with 150 entries compiled from a survey over 87% of the surface.
- Comparison between properties of the binary craters and the population of binary asteroid systems.
- Mismatch between observed and simulated properties of binary craters on Mars.
- Unobserved population of binary asteroids suspected with large separation, near-similar size, and non-zero obliquity

Evidence for widely-separated binary asteroids recorded by craters on Mars

Dmitrii E. Vavilov[a,b,*], Benoit Carry[a], Anthony Lagain[c], Anthony Guimpier[d], Susan Conway[d], Hadrien Devillepoix[c] and Sylvain Bouley[e]

[a] *Université Côte d'Azur, Observatoire de la Côte d'Azur, CNRS, Laboratoire Lagrange, France*
[b] *Institute of Applied Astronomy, Russian Academy of Sciences, St. Petersburg, Russia*
[c] *Space Science and Technology Centre, School of Earth and Planetary Sciences, Curtin University, Perth, WA, Australia*
[d] *Laboratoire de Planétologie et Géodynamique, UMR6112 CNRS, Université de Nantes, France*
[e] *GEOPS – Géosciences Paris Sud, Univ. Paris-Sud, CNRS, Université Paris-Saclay, Orsay, France.*

ARTICLE INFO

Keywords:
Asteroids, dynamics
Mars
Mars, surface
Cratering

ABSTRACT

Over the last decades, a significant number of small asteroids (diameter <10 km) having a satellite in orbit around them have been discovered. This population of binary asteroids has very specific properties (secondary-to-primary diameter ratio of about 0.3, semi-major axis to primary diameter ratio around 2 and an obliquity of the system close to either 0° or 180°) pointing at formation by YORP-induced spin-up and rotational fission. When impacting the surface of terrestrial bodies, those exotic objects lead to the formation of binary craters, exhibiting various morphologies depending on the configuration of the system at the moment of the impact. Planetary surfaces constitutes therefore the best (if not the only one) record of binary asteroid population through time. In contrast to the Moon or Mercury, a large fraction of impact craters on Mars exhibits thick ejecta layers due to the presence of volatile material at the moment of the impact (e.g., water ice). The martian surface represents thus the ideal case to survey for the existence of binary craters, as the ejecta morphology can attest of a synchronous impact. From a survey of 87% of Mars surface, we identify 150 binary craters (0.5% of the total), likely formed by the impact of binary asteroids. The properties of these craters contrast with those of the population of binary asteroids: size ratio close to unity, large separation, and isotropic orientation on the surface. We run numerical simulations of impacts to test whether tidal effects on the impact trajectory can explain these discrepancies. Our results suggest that a population of similarly-sized and well-separated binary asteroids with non-zero obliquity remains to be observed.

1. Introduction

Planetary surfaces not protected by dense atmospheres and without extensive geologic activity are covered by impact craters. Among these, about 3–4% have been estimated to be *binary* craters (Melosh et al. 1996), thought to form by the simultaneous impacts of the two components of binary asteroids. These have been found on almost every terrestrial surface in the inner Solar System including the Moon (Oberbeck 1973; Wren and Fevig 2020), Mars (Melosh et al. 1996; Miljković et al. 2013; Lagain et al. 2017, 2020), Venus (Cook et al. 2003), Ceres and Vesta (Fevig and Wren 2019), and one binary crater has even been reported on Tethys, a moon of Saturn (Chapman 2007).

On Earth, the high erosion rate removes morphological evidence preventing confirmation of a synchronous impact origin from a binary asteroid using the same technique as on extraterrestrial worlds. However, the similarity of radiometric ages associated with each crater of a potential binary constitutes the most convincing approach to confirm such origin. Among the 200 impact craters confirmed on Earth (Schmieder and Kring 2020), 12 (i.e., 6 binaries) craters have been suggested to have formed from a binary asteroid impact: Clearwater West and East, Kamensk - Gusev, Ries - Steinheim, Serra da Cangalha - Riachão, Lockne - Målingen and Suvasvesi North and South (see Schmieder et al. 2014, for a recent review). However, several of them are associated with ambiguous ages (Jourdan et al. 2012) and no binary craters have been confirmed on Earth (Schmieder and Kring 2020). Nevertheless, the Kamensk (25 km) – Gusev (3 km) and Lockne (7.5 km) - Målingen (700 m) crater pairs appear as very likely binaries owing to the correspondence between their respective revised radiometric age and superposition relationship for the former and high-resolution biostratigraphic dating for the latter (Schmieder and Kring 2020; Ormö et al. 2014). Although the population of most-likely binary craters on Earth is limited to two crater pairs only, it can be estimated that only about 1% of terrestrial impact craters might be formed by synchronous impact events.

The origin of these binary craters was originally debated as the existence of binary asteroids itself was disputed for decades (Weidenschilling et al. 1989). The discovery of Dactyl in orbit around (243) Ida by NASA *Galileo* (Chapman et al. 1995), followed by numerous discoveries of binary asteroids from the ground (by lightcurves, direct imaging, and radar, e.g., Pravec et al. 1997; Merline et al. 1999; Margot et al. 2002), revealed that asteroids do have satellites (Merline et al. 2002). It is now accepted that these binary craters result from the impact by binary asteroids (Miljković et al. 2013). It was originally thought that binary asteroids formed

*Corresponding author
vavilov@iaaras.ru (D.E. Vavilov); benoit.carry@oca.eu (B. Carry)
ORCID(s): 0000-0001-5242-3089 (B. Carry); 0000-0002-5391-3001 (A. Lagain); 0000-0002-4445-8123 (A. Guimpier); 0000-0001-9226-1870 (H. Devillepoix)

during close encounters with planet (Bottke and Melosh 1996). This has, however, been challenged by observations of binary asteroids in the asteroid belt (see Margot et al. 2015, for a review) and numerical simulations of close encounters (e.g., even the deep encounter of Apophis with the Earth in 2029 will not change its shape, see Yu et al. 2014).

From a photometric survey of near-Earth asteroids (NEAs), Pravec et al. (2006) derived a fraction of asteroids with satellites of $15 \pm 4\%$, for diameters larger than 300 m. The largest of these binary asteroids, discovered by either lightcurves or radar echoes, is (939) Isberga with a diameter of 13 km (Carry et al. 2015). This population of *small* binary asteroids has very specific properties: secondary-to-primary diameter ratio of 0.22-0.37 (25% and 75% quantiles), semi-major axis to primary diameter ratio of 1.7–2.8, obliquity close to either 0° or 180°, primary rotation close to spin barrier (2.5 h, e.g, Pravec and Harris 2007; Pravec et al. 2012; Harris et al. 2017). All these parameters, together with the large fraction of binary asteroids among asteroid pairs (Pravec et al. 2010), are evidence for a formation by YORP-induced spin up and rotational fission (Walsh et al. 2008; Walsh and Jacobson 2015). In recent years, another population of widely-separated binary asteroids has been announced from the observations of lightcurves presenting two distinct frequencies (Warner 2016; Warner and Stephens 2019). The properties (orientation, diameter ratio, separation) of these candidate binary systems are, however, largely unknown, as no mutual eclipses have ever been observed (Warner et al. 2018). By contrast, the population of 100+ km asteroids with small satellites detected by direct imaging (which incidence is estimated to a few percents only, Margot et al. 2015) has very different properties. These latter satellites are thought to form through collisions (Durda et al. 2004).

From 3-D numerical modeling of the impacts by binary asteroids, Miljković et al. (2013) showed that only a fraction of impacts by binary asteroids leads to the formation of binary craters on Mars. Depending on the size ratio of the components of the binary asteroids, and their physical separation at the time of impact, those objects create single craters in about 50% of the cases, otherwise leaving either doublet, peanut-shaped, tear-drop or elongated craters. These findings conciliate the apparent discrepancy between the fraction of binary asteroids (15%) and the reported 3–4% of binary craters (Miljković et al. 2013).

Considering the distribution of diameter ratio, semi-major axis to diameter ratio, and obliquity of the population of known binary asteroids (Harris et al. 2017), it is striking that most martian binary craters listed in Miljković et al. (2013, Table 2) display a diameter ratio close to one, a large separation, and may even be oriented along the North-South direction.

This raises the question of the origin of these binary craters. The discovery of satellites around small asteroids is achieved with radar echoes (among near-Earth asteroids only, Benner et al. 2015) or lightcurves (Margot et al. 2015). The latter are biased toward systems with either 0° or 180° obliquity and favor diameter ratio close to unity. Most detected systems have indeed a low obliquity (due to an anisotropic spin distribution clustering toward ecliptic poles, Pravec et al. 2006). The vast majority of these systems, however, clusters around a secondary-to-primary diameter ratio of 0.3, revealing a clear preference for this diameter ratio end-state for a formation by rotational fission (Walsh et al. 2008; Walsh and Jacobson 2015), with only a few exceptions (e.g., Benner et al. 2003). Similar-sized binaries are less common (diameter ratio above 0.5 represent 11% of current census only) and can present non-zero obliquities (e.g., (809) Lundia (1089) Tama, see Hanuš et al. 2013; Bartczak et al. 2017), albeit the statistics on pole coordinates is severely limited.

Planetary surfaces constitutes thus the best (if not the only) record of binary asteroid population through time. The recognition of separated doublet craters is more difficult without a clear continuous ejecta layer, which provides better evidence of a synchronous impact through the morphology. In contrast to the Moon or Mercury, a large fraction of impact craters on Mars exhibits thick and continuous ejecta blankets emplaced in a pyroclastic flow-like regime (e.g., Komatsu et al. 2007), as opposed to secondary materials ejected along a ballistic trajectory that form rayed and discontinuous ejecta blankets (e.g., Oberbeck 1975), due to the presence of volatile material at the moment of the impact (e.g., water ice). This facilitates the recognition of synchronous impact events (Lagain et al. 2017), making the surface of Mars an ideal case to survey for the existence of binary craters.

We study in the present article the characteristics of binary craters on Mars and compare them with numerical simulations of impacts. We describe in Section 2 our survey of binary craters on the surface of Mars and present the resulting catalogue in Section 3. We then describe in Section 4 numerical simulations to build the statistic of the orientation of binary craters based on the population of known binary asteroids. We finally compare the properties of the binary craters with the simulated geometries of impact and discuss implications in Section 5.

2. A survey of binary craters

We search the surface of Mars for impact craters exhibiting morphological evidences of multiple synchronous impacts. For this, we use the crater catalogue of Robbins and Hynek (2012a), revised by Lagain et al. (2021), in which the location, size, and morphology of impact craters larger than 1 km are compiled. Entries flagged as secondary craters (craters formed in the fallback collisions of ejecta from primary craters) are discarded. We also discard degraded structures as they did not retain morphological characteristics, such as their ejecta blankets, that might help in the identification of a binary crater. To limit the size of the sample investigated and ascertain in the binary origin of the impacts, we limit our focus on craters larger than 4 km in diameter and located between $\pm$ 50° of latitude, i.e., 31,778 entries (Figure 1).

We use the day-time Thermal Emission Imagery System (THEMIS) mosaic v12 (Edwards et al. 2011), offering

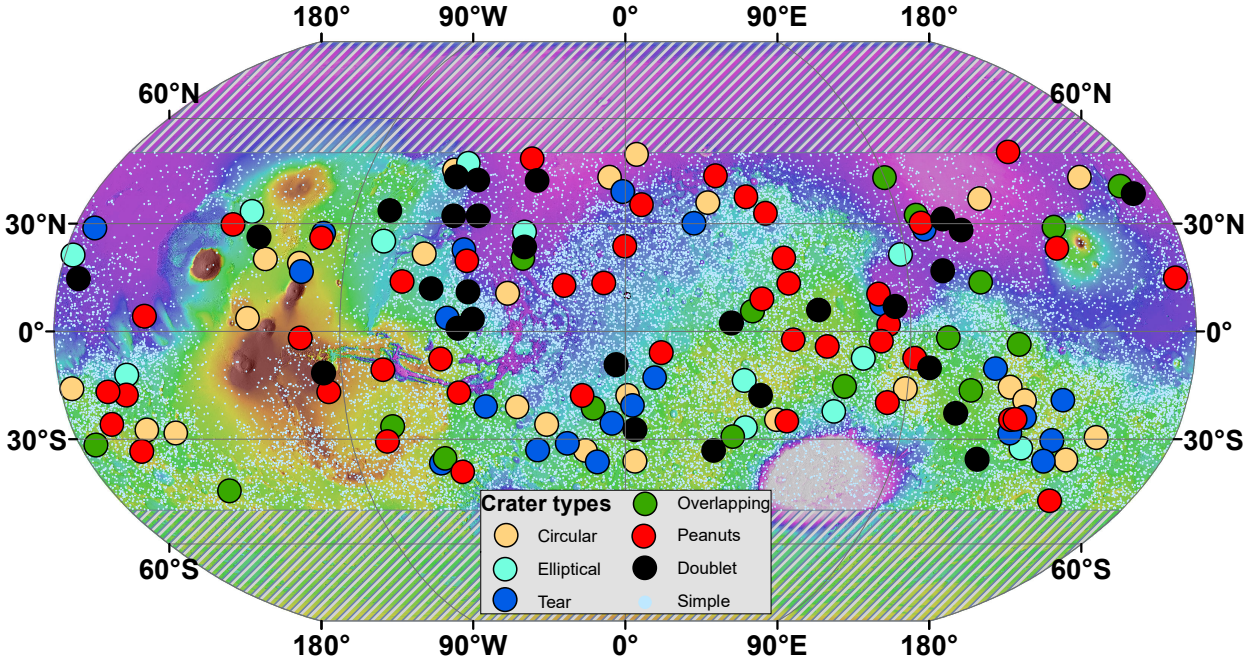

Figure 1: Distribution of impact craters larger than 4 km from Lagain et al. (2021) surveyed in this study, color-coded according to the classification proposed by Miljković et al. (2013). We focus on the equatorial region, between -50° and +50° of latitude. Background: topography of Mars based on the Mars Orbital Laser Altimeter mosaic (https://planetarymaps.usgs.gov/mosaic/Mars_MGS_MOLA_DEM_mosaic_global_463m.tif).

a global resolution of 100 m/px, and a semi-controlled CTX global mosaic, (6 m/px, Dickson et al. 2018). We conduct the survey to identify binary craters using Cesium Viewer[1], a Web platform adapted for the classification of geological features (Lagain et al. 2021). Craters determined to not likely be binaries are denoted by the small blue circles in Figure 1.

The diameter of each binary crater identified in our survey is then measured using the CraterTools module (Kneissl et al. 2011) available for ESRI ArcGIS as well as the distance between the centroid of both craters within a binary crater. Those properties allow to classify candidate binary craters following Miljković et al. (2013) classification based on their diameter ratio and separation:

- Doublet: this class is the only one where the ejecta blanket morphology allows the recognition of a potential doublet impact crater. The two components are sufficiently separated to preclude any contact between their rims. A bead (an excess of ejecta material) perpendicular to the axis defined by the two crater centroids is clearly visible between the respective ejecta blankets of the two components (Figure 2.a).

- Peanut: the two components of the potential binary are approximately of the same size and sufficiently separated to identify two distinct impact structures (without any evidence of a stratigraphic relationship) but still exhibit a contact (called a *septum*) between their rims (Figure 2.b),

- Overlapping: a minor impact crater is close but separated from the main binary component and does not exhibit a circular morphology, suggesting an overlap of material ejected from the main crater onto the minor crater following the impact event, when ejecta blankets are emplaced (Figure 2.c).

- Tear: a minor impact structure is adjacent (without any clear stratigraphic relationship) to the associated main crater (Figure 2.d),

- Elliptical: the impact crater is elliptical and the main direction of its ejecta blanket is perpendicular to the major axis of the crater cavity (Figure 2.e),

- Circular: Some impact parameters (small separation of both impactors and/or small diameter ratio) do not theoretically allow the formation of a binary crater (Miljković et al. 2013). We, however, mark as potential binary craters 25 circular craters based on the presence of a *septum* located on the central peak, or a partially circular structure on the rim (Figure 2.f). We anticipate a low confidence level in the binary craters identification falling into this category. We thus discard them from the analysis (but report them in the database).

[1] http://134.158.75.177/viewer/Apps/PlanetaryCesiumViewer/index.html

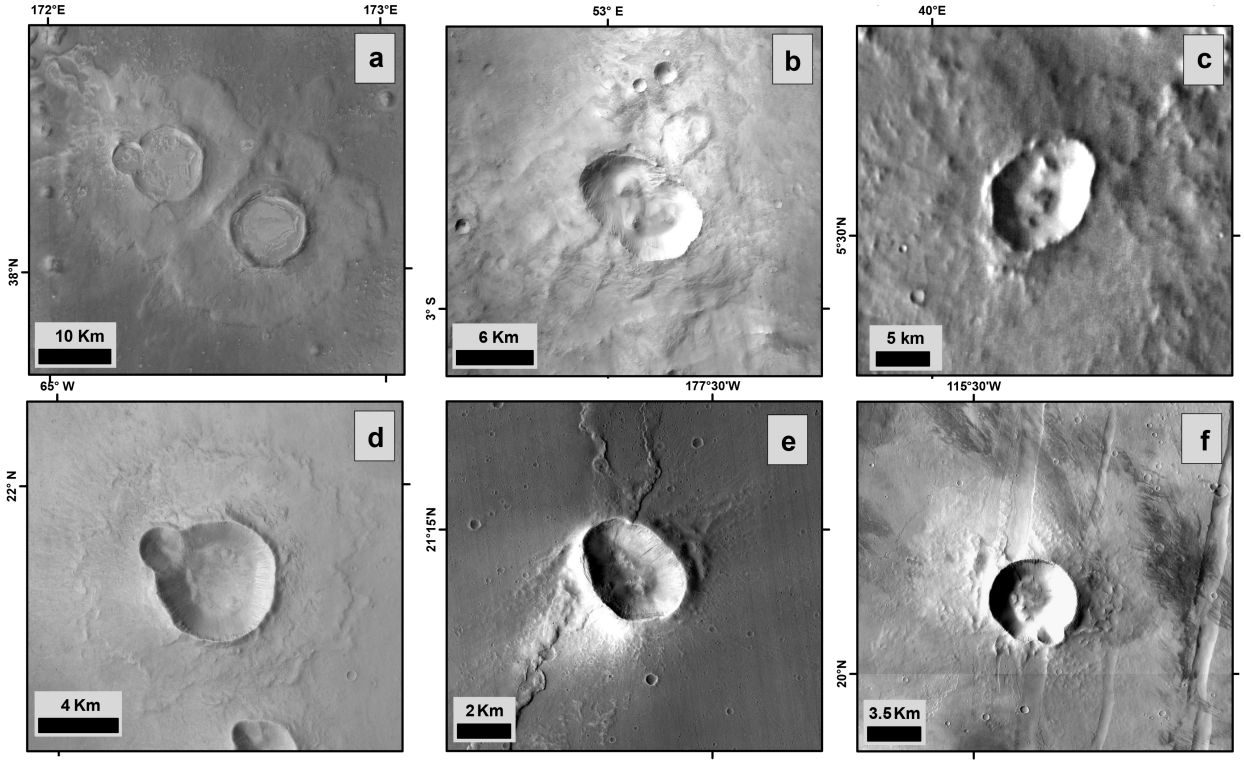

Figure 2: Example of impact craters classified as (a) doublet, (b) peanut, (c) overlapping, (d) tear, (e) elliptical and (f) circular seen with the CTX global mosaic (6 m/px, Dickson et al. 2018) and the THEMIS Day-IR mosaic v12 (100 m/px, Edwards et al. 2011)

. Craters presented on panels (a) and (b) present a *septum* (linear shared feature, respectively on the ejecta blanket and withing the cavity), attesting of an impact from a binary asteroid. Craters on panels (d) and (c) present one and wwo minor impact structures adjacent to the main impact crater, respectively. Panel (e) presents an elliptical impact crater without any visible forbidden zone. Panel (f) present a circular morphology with a minor impact structure on the south flank of the crater. The small separation between both structures makes this crater classified as circular following Miljković et al. (2013).

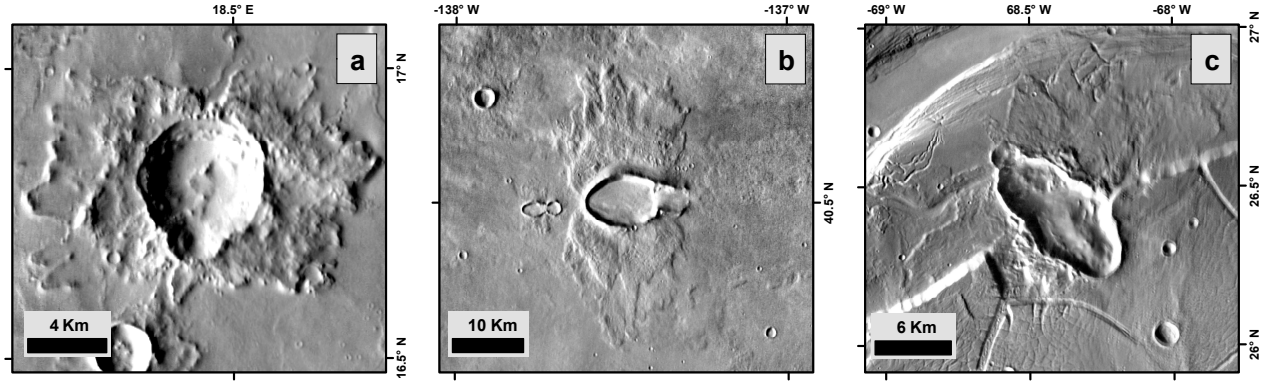

Figure 3: Example of impact craters formed in low-angle impact geometries seen with the THEMIS Day-IR mosaic v12 (100 m/px, Edwards et al. 2011): (a) This impact structure is similar to the one presenting in Figure 2.e, except that the forbidden zone at the North of the crater suggests that the small structure visible at the South of the main impact cavity originates from a grazing impact, (b) two distinct impact structures generated by ricocheting projectile, (c) highly elliptical impact crater formed under grazing regime (impact angle $\leq 5°$).

Besides the circular morphology the case of elliptical craters is the most arguable. 3-D hydrocode simulations and hypervelocity experiments demonstrated that they can be formed by both binary asteroid impacts or single asteroids under low-angle impact conditions (Elbeshausen et al. 2013; Gault and Wedekind 1978). While craters formed by a single asteroid impacting the surface with an angle of 20° will exhibit an elliptic geometry, lower impact angles might lead to the partial or the total decapitation of the projectile (depending in the impact angle and cohesion of both the target and the projectile) and form successive impact craters in the direction of the impact, exhibiting limited eccentricity (Figure 3, Elbeshausen et al. 2013). In such grazing impacts, a *forbidden zone* (i.e., an area lacking ejecta) at the back of the impact constitutes one of the most convincing morphological evidence to distinguish between low-angle single asteroid and binary asteroid impact.

3. Properties of binary craters on Mars

Out of the 31,778 craters we inspected, we identify 28 doublet, 44 peanut, 17 overlapping, 23 tear, and 13 elliptical craters (Figure 1). We note that 25 further potential candidates have been identified and are classified as circular according to Miljković et al.'s scheme. This brings the total number of binary crater candidates to 150 (300 individual) corresponding to 0.5% of the total surveyed population (see Appendix A for the complete list of craters with their characteristics). Although the results of numerical simulations by Miljković et al. (2013) predict a theoretical impossibility to identify binaries from circular craters, morphometric measurements (crater diameter ratio and separation) of these 25 craters fit with this class characteristics defined by Miljković et al. (2013). This conflict can be explained by a misclassification of the morphometric measurements for circular binaries in our survey, a variability of morphologies depending on the impact conditions (impactor size, impact angle and velocity, cratering efficiency...) not identified by the numerical simulations, an approximation of the resulting morphology due to the simulation resolution, or a combination of these factors. We also note that the classification proposed by Miljković et al. (2013) we use in this study is based on discrete parameters thresholds defining each category. In the reality, a variability of such limits due to impact parameters mentioned above might exist, thus nuancing the resulting crater morphologies and classification.

The degradation state of impact features investigated here leads to an unclear binary asteroid impact origin for a non-negligible number of cases. Thus, the completeness of the binary asteroids record on the surface of Mars cannot be assured in this work, whatever the morphological class considered. In this regard, our attempt to determine the proportion of binary systems in the asteroid population based on impact craters can only provide a lower limit.

We also estimate the projectiles diameter that formed each crater identified in our survey using the scaling laws described in Collins et al. (2005):

$$D_t = 1.161 \left(\frac{\rho_i}{\rho_t}\right)^{\frac{1}{3}} L^{0.78}\, v_i^{0.44}\, g^{-0.22}\, sin^{\frac{1}{3}}(\theta) \qquad (1)$$

where D_t is the diameter of the transient crater, ρ_i and ρ_t are respectively the density of the impactor (taken as 1.9 g/cm^3, the density of asteroid Itokawa, typical for small asteroids, Fujiwara et al. 2006; Carry 2012) and the target (3.0 g/cm^3, Archinal et al. 2018), L is the impactor size, v_i is the impact velocity at the surface, g the Martian gravitational acceleration, and θ the impact angle (45°). The diameter of the transient crater is then used to estimate the diameter of the final crater (D_f), and by inversion, the impactor diameter related to each crater of the survey:

$$D_f = \begin{cases} 1.17\,\dfrac{D_t^{1.13}}{D_c^{0.13}}, & \text{if } D_t < D_c; \qquad (2) \\ 1.25\,D_t, & \text{if } D_t > D_c. \qquad (3) \end{cases}$$

where D_c is the transition diameter between simple and complex craters, estimated to 6 km (Robbins and Hynek 2012).

The impact craters we measured here (D_m) range between 1.5 km $< D_m <$ 40.5 km. Calculations suggest they were produced by binary asteroids ranging between 70 m and 3.8 km.

The population of craters we identify strongly contrasts with the population of known binary asteroids in both separation[2] and diameter ratio (Figure 4). This is partly due to the biases affecting the detection of binaries among both asteroids and craters. Compact asteroid systems are more easy to detect, while close-in craters are not. Nearly-similar sized component are, however, easier to detect in both populations. This nevertheless suggests that widely separated binary asteroids exist, even if little have ever been detected with a separation above four primary diameters. Indeed, Melosh and Stansberry (1991) studied the impact of contact-binary asteroids with planetary surfaces and found that the physical separation was not significantly affected by tidal forces.

We illustrate the geometry of the 112 doublet, peanut, overlapping, and tear-drop craters in Figure 5 (circular and elliptical classes orientation lead, by definition, to a higher uncertainty in the orientation measurement). As suspected from the craters listed in Miljković et al. (2013, Table 2), the orientation of the craters appears isotropic, without a preferential direction. This is quite surprising considering the anisotropic distribution of orientation of known binary asteroids (Pravec et al. 2006) and we focus on this aspect in the following section.

4. Orientation of binary asteroid impacts

Melosh and Stansberry (1991) studied the impact of contact-binary asteroids with planetary surface but did not discuss

[2] The physical separation of the two components of the binary system is the same as the crater separation, as computed by Melosh and Stansberry (1991).

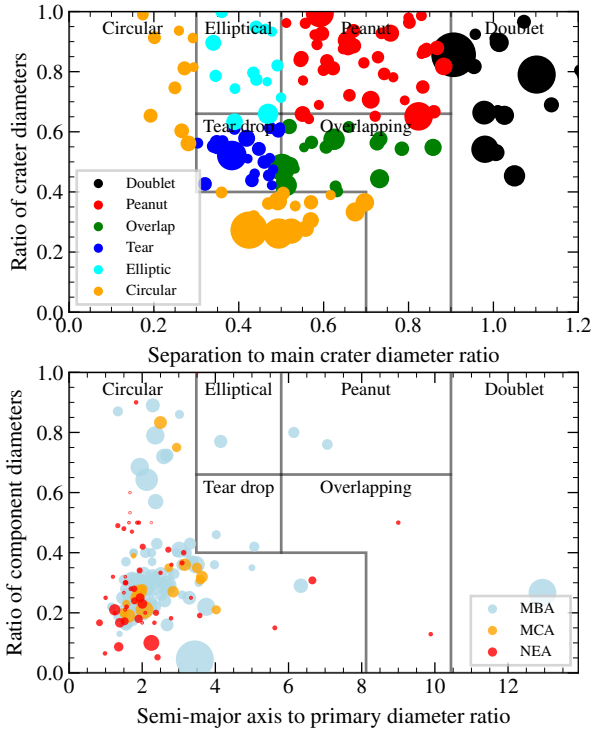

Figure 4: Distribution of craters (top) and binary asteroids (bottom) in semi-major axis and size ratio space, color-coded according to their orbital characteristics (Main Belt Asteroids (MBA), Mars-Crossing asteroids (MCA), and Near-Earth Asteroids (NEA)). The rectangular regions indicate the crater types defined by Miljković et al. (2013), scaled by a factor of 11.6 in the bottom plot (the average of all scaling factors from Equation 4). The size of symbols is representative of the diameter of the main components.

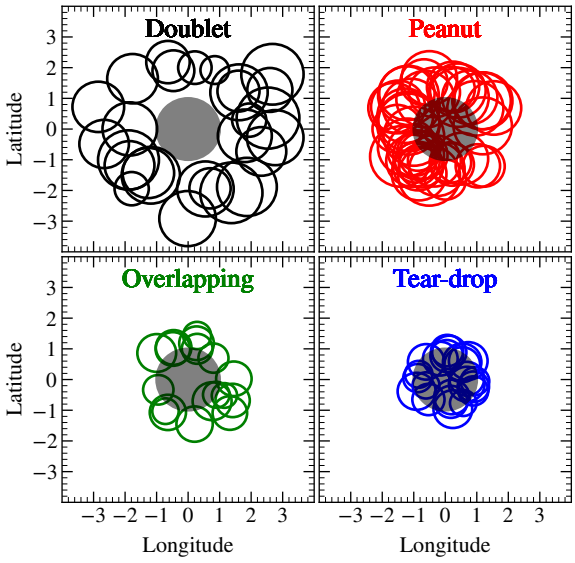

Figure 5: Geometry of doublet, peanut, overlapping and tear-drop craters. The axes are parallel to the longitude and latitude on Mars surface, centered on the primary crater, and normalized to its radius. The primary crater is represented by the central grey disk, and the secondary craters are represented at their scaled location and diameter.

the orientation of impacts (with respect to the equator of Mars). We estimate in the present section the distribution of the orientation of binary craters as expected from the current census of binary asteroids.

4.1. Geometry of encounter

We first study the geometry of impact of binary asteroids on a Mars without accounting for its gravitational attraction.

We consider all the asteroids with a Minimal Orbital Intersection Distance (MOID, Marsden 1993) with the orbit of Mars smaller than 0.05 au (i.e., Mars-crossing and near-Earth asteroids only). That is we consider only asteroids that have a reasonable possibility of colliding with Mars. We retrieve the orbits of Mars and the asteroids from JPL[3].

We assume that a collision takes place at the MOID point: the location in space where the orbits of the asteroid and Mars are the closest to each other. We compute the MOID points using the method of Baluyev and Kholshevnikov (2005).

We define the orientation θ of the double impact (resulting for the impact of the two components of the binary asteroids) on Mars surface as the angle between Mars' equator and the line connecting the center of the two craters. For that, we use the IAU definition of the north pole orientation of Mars, (RA,Dec) = (317.3°, +54.4°), from Archinal et al. (2018).

We assume here that the mutual orbit of each binary asteroid system is circular, and coplanar with its heliocentric orbit (i.e., their obliquity is null). This choice is imposed by the anisotropic distribution of spins among the population of known binary asteroids (clustering around 0 and 180° obliquity, see Pravec et al. 2012) and it is expected for a formation via YORP spin-up and rotational fission (Walsh et al. 2008; Pravec et al. 2010).

We compute the orientation angle θ as follows. We place Mars and the binary asteroid at their MOID point, and compute their relative velocity:

$$\mathbf{v} = \mathbf{v_b} - \mathbf{v}_{\sigma}$$

where $\mathbf{v_b}$ is the Keplerian velocity of the center mass of the binary, and $\mathbf{v}_{\sigma}$ the Keplerian velocity of Mars (the relative velocity are typically within 5 to 15 km/s). We construct the target plane as the plane perpendicular to the relative velocity, $\mathbf{v}$, containing the center of Mars (Kizner 1961). We project the positions of the two components of the system on the target plane. The angle θ is the angle between the line connecting the projection of the two components and

[3] Mars: http://ssd.jpl.nasa.gov/txt/p_elem_t2.txt
Asteroids: http://ssd.jpl.nasa.gov/sbdb_query.cgi

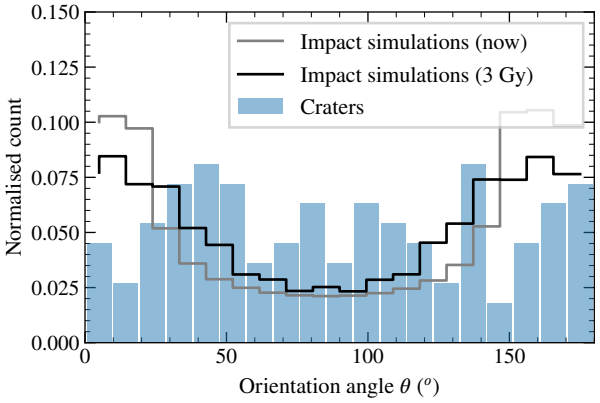

Figure 6: Distribution of crater orientation (Section 3) and simulated impacts (Section 4), for both current obliquity of Mars and integrated over 3 Gy.

Figure 7: Geometry of the numerical simulations. The components of binary system of masses M_1 and M_2 are targeted on Mars with an inclination i, a velocity $\mathbf{V}$, at an impact parameter p.

the projection of the equator of Mars on the target plane. To account for the unknown orbital phase of the binary systems at the epoch of impact, we sample their mutual orbit by 360 positions, and compute θ for each.

We present in Figure 6 the probability density function (PDF) of the orientation angle θ for the current obliquity of Mars. The spin-axis of Mars has, however, wandered in the past (with excursions of 60°, see Laskar et al. 2004). Variations in the spin axis imply a changing obliquity which smoothens the peak of the distributions. The oldest binary craters in our survey is about 3 Gy old. The analysis of elliptical craters distribution from Holo et al. (2018) suggests that Mars' mean obliquity was likely between 10° and 30° over the last 3.5 Gy, and the fraction of time spent at obliquities >40° was likely below 20%. We thus need to account for this spin evolution to quantify the potential smoothing of the orientation angle distribution of binary craters.

The obliquity of Mars is unpredictable over long time intervals, as it is chaotic (Laskar et al. 2004). From multiple simulations of the spin orientation history of Mars, Laskar et al. (2004) showed that its obliquity follows a Gaussian distribution with an average of about 37°, and a standard deviation of 13° (the latter increases the longer the time period considered, see their Table 5). This range of obliquity is broader than estimated by Holo et al. (2018). We choose it as a conservative baseline: the broader obliquity distribution will indeed smooth the predicted distribution of crater orientation more than a narrow distribution. Assuming the properties of the population of binary asteroids did not evolved over time (YORP-induced formation produces zero obliquity systems, Walsh et al. 2008), we build the PDF of the orientation angle θ over 3 Gyrs by summing the distributions obtained for different values of the obliquity, weighted by the aforementioned Gaussian distribution of obliquity.

We report this PDF of orientation in Figure 6. The predicted distribution of orientations presents a broad plateau along the East-West direction. For each North-South binary crater on Mars, there should be three more along the East-West direction if binary systems have zero obliquity. This is clearly at odd with our census of craters (Figure 5). Because we chose the broader distribution of obliquity, these results are robust and would be more pronounced if the excursion of Mars obliquity had been more limited (e.g., Holo et al. 2018).

Finally, True Polar Wander episodes on Mars, i.e. the crust motion with respect to the spin axis induced by a mass redistribution, might have influenced the binary craters orientation over time. However, mass redistributions on the surface of Mars induced by volcanic activity did not occur during the Amazonian (over the last 3 Gy, which correspond to the oldest binary crater identified here) but most likely during the Hesperian (Kite et al. 2009; Bouley et al. 2016). It is therefore unlikely that such mechanism contributed to a significant attenuation, or more generally, to the modification of the binary asteroids record on Mars.

4.2. Tides-induced change of geometry

The computation presented above neglects the differential gravitational attraction of the target on the components of the binary systems. This is due to the lack of constraints on the exact geometry of impacts, mainly the impact parameter, p (the distance between the barycenter of the planet and the asteroid velocity vector) and the impact angle (the angle between the surface and the asteroid velocity vector). However, we now explore this using a Monte-Carlo approach to gauge any potential influence.

We study in this section the change of orientation $\delta\theta$ due to the target gravity, focusing on Mars. This is an extension of the work by Melosh and Stansberry (1991) who noted that the separation was only marginally affected.

We consider the following three-body problem (Figure 7). The center of the coordinate system coincides with the barycenter of Mars, which is assumed to be a sphere with a radius of 3389 km (Archinal et al. 2018). We integrate the motion of the binary asteroid from a distance of 0.1 au to its impact on Mars. The center mass of the binary asteroid is originally set at $(-0.1, 0, p)$ au, where p is the impact parameter. The direction of the initial velocity $\mathbf{V}$ is parallel to the x-axis. We use three typical values of the relative velocity (5, 10, 15 km/s, Table 1) between the impactor and Mars, derived from the simulations in Subsection 4.1. We do not consider larger velocities since the effect decreases with increasing relative

Table 1
Values of the different parameters used in the numerical integrations (see text).

	Considered values	Unit
V	5, 10, 15	(km/s)
M_1	$10^9, 10^{10}, 10^{11}, 10^{12}, 10^{13}, 10^{14}, 10^{15}, 10^{16}$	kg
γ	1,2,4,6,8,10,20,30,40,50,60,70,80,90,100	%
T	12, 24, 36, 48, 240	hours
p	-0.9, -0.5, 0, 0.5, 0.9	R_{target}
i	0, 45, 90	°

velocity.

We explore a wide range of parameters for the impact of binary systems (Table 1):

- M_1, the mass of the primary component, taken from 10^9 kg to 10^{16} kg. The lower bound corresponds to a diameter of 100 m, leading to a crater of about 1 km, the typical size for completeness in crater catalogues (Robbins and Hynek 2012a,b). The upper bound encompasses the largest known small binary, (939) Isberga (Carry et al. 2015).
- $\gamma = M_2/M_1$, the mass ratio between the components, sampled from equal masses ($\gamma = 1$) to satellites about five times smaller than the main component ($\gamma = 0.01$).
- T, the period of the mutual orbit of the binary, sampling the typical period of 24^{+24}_{-12} h (Harris et al. 2017), and a long period of 10 days for well-separated binaries, such as the widely separated population (Warner et al. 2018).
- p, the impact parameter describing the distance between the velocity vector of the binary and the center of Mars, in units of Mars radius (R_{target}).
- i, the inclination between the orbital plane of the binary and its velocity **V**, sampling coplanar, perpendicular, and oblique impacts.

We assume that the binary orbit is circular at the start of the integration. We sample the respective positions of the components on their mutual orbit by 360 initial positions. We propagate the positions of the two components using the 15$^{\text{th}}$ order numerical integrator by Everhart (1985) until the components collide with Mars at t_{imp}. If both components collide with Mars, we compute the angle θ_p between the line connecting the location of the components and the equator.

To estimate the change of orientation $\delta\theta$, we estimate θ, the orientation of the binary crater for each simulation, without the perturbation induced by Mars. The unperturbed coordinates of the components at time t_{imp} are determined from their orbital period T and their Keplerian relative velocity (**V**). We project their positions on the target plane (perpendicular to the relative velocity, hence the yz-plane), and compute the angle between the line connecting the projections, and the equator.

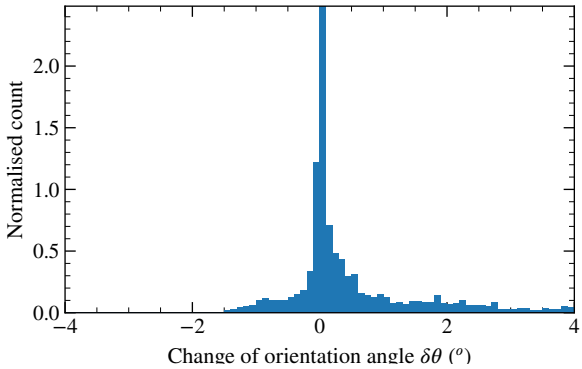

Figure 8: Histogram for the change of orientation $\delta\theta$ for Mars. The standard deviation is 0.72°.

Hence, each combination of simulation parameters in Table 1 is sampled 720 times: 360 perturbed angles ($\{\theta_{p,i}\}_{i=1}^{360}$) from the numerical propagation and 360 unperturbed angles ($\{\theta_i\}_{i=1}^{360}$), resulting in 1,944,000 outcomes. From these, we remove those for which the impacts are located too far from each other to be recognized as doublet craters. We set a threshold distance of 100 km. Similarly, we remove impacts too close to each others, leading to circular craters. Following the work of Miljković et al. (2013), we set a threshold distance of three times the diameter[4] of the primary component.

We compute the change of orientation $\delta\theta$ as

$$\delta\theta = \min_{k=0,\dots 359} \max_{i=1,\dots 360} |\theta_{p,i} - \theta_{[i+k]}| \quad (4)$$

where $[i+k] = mod(i+k, 360)]$, and only using i indices not rejected based on the aforementioned distance thresholds. We thus search for the maximal change of orientation, but removing aliases in which the two components impact Mars with the same orientation as another k sampling of their mutual orbit. We find the k from Equation 4 and compute the difference of angles $\delta\theta$.

The distribution of the change of orientation $\delta\theta$ is presented in Figure 8. The distribution is strongly peaked around 0°, with a standard deviation of only 0.72°. These simulations imply that the orientation of binary crater is not significantly affected by the tidal forces, similarly to their separation (Melosh and Stansberry 1991). This confirms the discrepancy between the anisotropy observed among binary asteroids and the isotropic distribution of orientation of binary craters.

5. Discussion

The numerical simulations indicate that the separation and orientation of the impacts by binary asteroids are not significantly affected by Mars (Section 4 and Melosh and Stansberry 1991). There are hence binary asteroids whose

[4] estimated from its mass as $d = \sqrt[3]{3M_1/(4\pi\rho)}$, where the density ρ is set to 1.9 g/cm^3 (like Itokawa, Fujiwara et al. 2006).

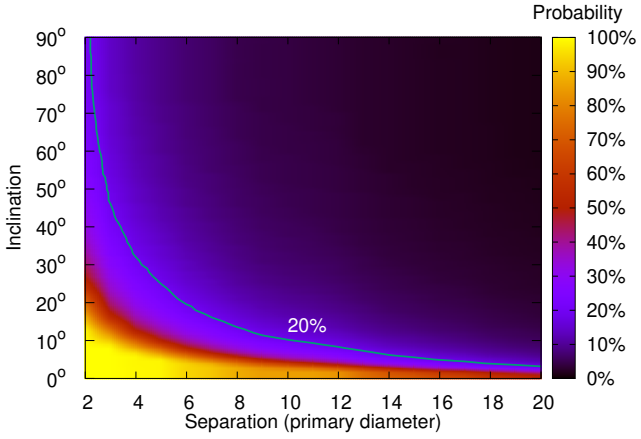

Figure 9: Probability of detecting mutual events of binary asteroids as a function of their inclination and separation. The blue isoline refers to 20% probability level.

separation is larger than those currently observed: indeed, the separation at impact is only a fraction of the semi-major axis (because separation is just a projection). The distribution of separation here is only a lower limit to the distribution of semi-major axes. Furthermore, in the range of diameter (0.2–4 km), diameter ratio (0.4-1.0), and separation (3–14 diameters) observed here, the binary asteroids do not appear to present coplanar orbits with their heliocentric orbits (as opposed to the distribution of most known binary asteroids, see Pravec et al. 2006). We perform a Kolmogorov-Smirnov test on the two distributions of observed craters and expected impact orientations from the known population of binary asteroids (Figure 6). We can reject with a 95% confidence that the two distributions are similar.

While drawing a distribution of mutual orbit parameters (inclination, longitude of the ascending node, pericenter, eccentricity and semi-major axis) that would reproduce the observed distribution of binary crater orientations is appealing, we restraint from doing so. This exercise is an ill-posed problem, and many 5-D distributions may match the 1-D distribution of crater orientation. We thus cannot predict a unique distribution of orbital parameters of binary asteroids, but can assert that it must not be comprised solely of objects whose mutual orbit is coplanar with their heliocentric orbit.

The question is therefore why such type of binary systems have not been detected yet. All the systems are too small (below 3.8 km, see Section 3) for having been directly imaged. Ground-based telescopes equipped with adaptive-optics (AO) require a bright source to close the AO loop (e.g., Merline et al. 1999; Marchis et al. 2006; Margot and Brown 2003; Carry et al. 2011; Pajuelo et al. 2018; Marsset et al. 2020), and the Hubble Space Telescope targeted the largest main-belt asteroids only (e.g., Storrs et al. 1999, 2005; Thomas et al. 1997, 2005).

While stellar occultations can detect satellites through secondary events (Timerson et al. 2013; Berthier et al. 2014), observations are challenging for small targets as the duration of the blink-out event is directly related to the diameter of the asteroid. Furthermore, with current prediction capabilities, the uncertainty on the location of the narrow occultation path on Earth is much larger than the shadow path itself, making the observation of such event very difficult (Tanga and Delbo 2007; Ferreira et al. 2020) As a result, 90% of the recorded occultations available at the Planetary Data System (Dunham et al. 2017) were obtained for asteroids larger than 45 km, and the smallest for a 4 km asteroid: (1685) Toro.

Most binary asteroids were discovered by optical light curves, especially in the asteroid belt (see Johnston 2018). The observability of mutual eclipses and occultations is, however, strongly dependent on the system parameters, and in particular its orientation. The more separated and inclined the binary, the more difficult it will be to detect it by optical lightcurves. We present in Figure 9 the computed probability of distinguishing a binary asteroid from a single one as function of the separation between the components and the inclination of their mutual orbit. This is simulated for a binary asteroid on a heliocentric circular 2.2 au orbit, inclined by 4° on the ecliptic plane. The probabilities are averaged obtained by sampling diameter ratio (from 0.3 to 1), density (1,000 to 3,000 kg.m^{-3}), longitude of ascending node of binary orbit (0–360°), and the initial position of the satellite (0–360°). It was assumed that the object is observed over 8 consecutive nights during 6 hours each, as an illustration of a dedicated search program for asteroid satellites. System separated by more than 4–6 primary diameter and inclined by more than 5–10° will probably be categorized as a single asteroid because no mutual event will be recorded (see the discussion by Warner et al. 2018).

Radar observations contributed to more than half of the discoveries of binary systems among near-Earth asteroids (see Johnston 2018). These observations are not biased toward low-inclination binary systems, and could easily detect wide and inclined systems (Brozović et al. 2011; Shepard et al. 2006; Ostro et al. 2005). However, the steep decrease of the echo power as function of the distance to the power of -4 precludes radar observation of small main-belt asteroids (only some of the largest were targeted, e.g., Shepard et al. 2018; Ostro et al. 2010). Furthermore, the population of NEAs is the result of a strong selection effect: most NEAs originate from the inner main-belt through the ν_6 resonance (Bottke et al. 2002; Granvik et al. 2017). The asteroids reach this resonance through an inward drift induced by the Yarkovsky effect (Vokrouhlický et al. 2015). As a result, the population of NEAs is comprised of asteroids presenting an excess of large-obliquity, retrograde rotators (La Spina et al. 2004). Most NEAs are thus oriented in a configuration favorable to YORP spin-up and formation of satellites by rotational fission (Walsh et al. 2008) even before their injection into the near-Earth space. These YORP-formed binary systems should hence dominate the sample of NEAs with satellites (15%, Pravec et al. 2006).

Hence, the binary craters we observe on Mars reveal a small population (0.5%) of widely separated (more than 10 primary diameters) and near-similar sized (median diameter ratio of 0.7) binary asteroids in the main belt with randomly

distributed mutual orbits. Taking into account the small incidence of this population and the limitations of the different observing methods used to detect binary asteroids, it is not surprising that none has been observed yet. Several mechanisms may be invoked to create such systems, and we describe them here below.

These binary asteroids could be remnants of a catastrophic collision between two asteroids called Escaping Ejecta Binaries (EEB) described by Durda et al. (2004). Predicted more than a decade ago, these EEBs have never been detected with maybe the sole exception of (317) Roxane (Drummond et al. 2021). Their size ratio is predicted to be bimodal, peaking at 0.05 and 0.55. While the former have satellites too small to be detected by our crater survey, the latter corresponds to the craters we observe. These EEBs should not present any preferred orientation during their formation. They also have significant eccentricity and Lidov-Kozai oscillations (Perets and Naoz 2009) will further randomize the inclination on short time scales (tens of years). This mechanism does not explain, however, the predominance of fast-rotating asteroids among the candidate widely-separated binaries (Polishook et al. 2011).

Alternatively, these binary asteroids could be the direct outcome of the fission triggered by YORP spin-up. While most systems simulated in numerical experiments mimic the observed population of small binary systems (Walsh et al. 2008), some low-mass ratio systems may be produced (Jacobson and Scheeres 2011). While most of them are unbound (becoming pairs of asteroids, Pravec et al. 2010), the YORP spin-up and fission may create a limited number of nearly equal-sized systems, more separated than the typical couple of primary diameter (Jacobson and Scheeres 2011). This mechanism would, however, preferentially create systems which mutual orbit is coplanar to their heliocentric orbit.

An alteration mechanism, put forward very early as potentially responsible for the formation of binary system (Bottke and Melosh 1996), may also be at play: planetary encounters (Fang and Margot 2012). Planetary flybys may excite the mutual orbit of a system, inclining and expanding it. Several wide-binary candidates are, however, found in non-planet crossing populations (Jacobson et al. 2014), and this alteration mechanism cannot be the sole responsible.

Finally, these binary asteroid systems may result from a complex, yet natural for irregular-shaped bodies, chain of processes, including the binary Yarkovsky - O'Keefe - Radzievskii - Paddack (BYORP) effect (Jacobson et al. 2014). This latter hypothesis may explain the size ratio, wide separation, fast-spinning, and seemingly ubiquitous presence of wide binaries among different dynamical populations. It does not, however, explain the apparently random orientation of the orbits reported here.

6. Conclusion

We conducted a survey of binary craters on Mars surface located between -50 and +50 degrees of latitude. From 31,778 craters larger than 4 km in diameter we identified 150 binary craters plausibly produced by binary asteroids. These are typically similarly-sized impacts, widely separated, and randomly oriented on the surface of Mars.

From numerical simulations we computed the statistical properties of binary craters predicted from currently known properties of binary asteroids. We showed that gravitational perturbation from Mars does not considerably change the inclination of the binary mutual orbit before impact, adding to previous work showing that the separation is also not affected (Melosh and Stansberry 1991). Thus the results of our numerical simulations without gravitational influence can be compared to the observed properties of binary craters.

We found a striking discrepancy between the properties of observed binary craters and those predicted from the current census of binary asteroids: observed craters are randomly oriented and more widely separated, while most known satellites of asteroids have tightly clustered properties (close-in orbit, coplanar with the heliocentric orbit).

This implies that there is a population of similarly-sized and well-separated binary asteroids with non-zero obliquity of their mutual orbit with respect to their heliocentric orbits. They may correspond to the few wide binaries recently reported by, e.g., Warner (2016) and Warner and Stephens (2019). The limited observations of these objects may be explained by the very low probability of detecting these systems with current observing techniques Warner et al. (2018).

Acknowledgments

B. Carry acknowledges support by the French ANR, project T-ERC SolidRock (ANR-20-ERC8-0003). A. Lagain is funded by the Australian Research Council (DP170102972 and DP210100336).

A. Catalog of binary craters

We list here the properties of craters identified as resulting from the impact of binary asteroids. c1 and c2 are associated respectively with the parameters of the largest and smallest crater of the binary. X and Y are respectively the longitude and latitude of the considered crater, D, its diameter in kilometers, the *distance* is the separation in kilometers between the crater centroids of the binary crater and *az_N* is the orientation of the binary crater measured from the angle made by the line linking the centroid of both craters relative to North. The *class* corresponds to the morphological classification according to Miljković et al. (2013): 1 = circular, 2 = elliptical, 3 = tear, 4 = overlapping, 5 = peanuts and 6 = doublet (see main text for more details).

X_c1	Y_c1	D_c1	X_c2	Y_c2	D_c2	class	distance	az_N
-123.8	33.311	4.1918	-123.83	33.326	2.9913	2	2.0942	294.77
-78.191	33.555	10.052	-78.116	33.752	7.965	6	12.233	17.429
-30.375	41.993	40.482	-31.204	42.657	21.973	6	53.484	317.32
-5.3415	42.882	17.289	-5.2973	42.733	4.6634	1	9.0476	167.76
-58.62	43.035	9.241	-58.343	42.935	6.6115	6	13.353	116.17
-33.242	48.11	7.9615	-33.37	48.081	7.0542	5	5.337	251.16
-59.951	44.947	6.8672	-59.981	44.939	4.4879	1	1.3198	249.66
-55.648	46.815	5.6635	-55.621	46.853	4.3812	2	2.4996	25.765
-0.73242	38.909	5.3808	-0.72929	38.952	2.4483	3	2.535	3.2494
-56.606	32.12	5.0533	-56.607	32.245	4.5375	6	7.3692	359.67
-50.834	42.081	5.1301	-50.937	42.01	4.1281	6	6.1768	227.07
-48.588	32.139	4.0756	-48.569	32.319	3.8033	6	10.705	5.1697
4.2106	49.458	22.592	4.0944	49.631	5.9086	1	11.157	336.42
27.716	35.727	10.83	27.719	35.599	3.9547	1	7.5482	178.92
5.5733	35.282	10.183	5.4922	35.385	7.196	5	7.2393	327.3
40.856	37.398	6.7498	40.77	37.432	6.3166	5	4.5244	296.31
31.465	43.339	5.8542	31.406	43.399	4.6397	5	4.3476	324.22
22.499	29.972	9.1436	22.537	30.023	5.7913	3	3.5666	32.972
46.599	32.793	3.7832	46.644	32.826	2.6653	5	2.9928	49.221
104.8	31.295	13.408	104.91	31.077	6.0803	6	14.075	156.27
90.047	42.768	9.5453	90.079	42.687	4.6563	4	4.9709	163.95
119.44	36.922	8.806	119.33	36.916	2.6921	1	5.0151	265.86
97.18	30.124	4.5177	97.126	30.079	3.9676	5	3.8064	226.25
96.311	32.276	3.6662	96.34	32.255	1.7486	4	1.9513	130.98
157.81	42.893	30.471	157.94	43.089	8.3169	1	12.929	25.906
169.49	40.331	14.115	169.57	40.438	5.9572	4	7.2124	28.946
172.35	38.254	10.411	172.65	38.097	10.291	6	16.74	123.7
139.16	50.016	7.073	139.13	49.945	5.7386	5	4.399	196.1
-173.83	14.634	11.518	-174.12	14.564	9.4488	6	16.935	255.77
-173.46	28.766	9.3827	-173.52	28.72	5.4275	3	3.9273	226.52
-151.67	4.2218	4.7448	-151.63	4.1947	4.2238	5	2.773	125.31
-177.55	21.214	3.4106	-177.57	21.235	2.6151	2	1.5921	320.98
-118.93	26.191	6.8143	-119.06	26.249	6.5831	6	7.3051	298.04
-128.53	29.702	6.7932	-128.59	29.786	5.902	5	5.6951	330.26
-98.514	25.967	6.453	-98.441	26.033	4.3018	5	5.5486	44.837
-98.268	27.263	6.1375	-98.225	27.272	3.207	3	2.294	76.336
-115.43	20.084	5.5305	-115.41	20.048	1.7629	1	2.4077	153.16
-104.31	18.966	5.117	-104.29	18.966	5.0653	1	0.89062	89.607
-119.07	3.589	3.9496	-119.04	3.6179	1.5381	1	2.4346	45.3
-103.3	16.6	3.804	-103.28	16.619	1.606	3	1.8176	53.286
-61.516	11.855	31.547	-62.023	12.171	24.935	6	34.762	302.47
-49.786	11.01	11.301	-49.596	11.062	10.135	6	11.456	74.284
-48.096	3.3733	11.682	-48.068	3.6462	10.483	6	16.228	5.7702
-52.62	0.83534	7.8112	-52.662	0.69131	5.3867	6	8.879	196.33
-64.648	21.514	6.3906	-64.699	21.541	2.5253	1	3.2245	300.12
-70.942	13.814	4.7237	-70.925	13.773	4.5385	5	2.6302	157.97
-78.168	25.086	5.7379	-78.199	25.117	4.5688	2	2.4924	318.12
-51.886	22.635	5.4881	-51.859	22.608	3.3492	3	2.1398	136.6
-56.171	3.6448	4.0341	-56.138	3.653	2.4794	3	2.0048	76.041
-50.66	19.525	4.076	-50.692	19.55	2.6189	5	2.3044	309.28
-37.227	10.521	10.664	-37.311	10.554	3.9382	1	5.2473	291.57
-32.755	20.251	9.6121	-32.66	20.358	5.2688	4	8.2455	39.468
-19.345	12.804	5.1039	-19.294	12.764	4.7342	5	3.7573	128.58
-32.781	27.608	4.4419	-32.767	27.635	3.3032	2	1.7368	24.19

Continued on next page

Table2 – continued from previous page

X_c1	Y_c1	D_c1	X_c2	Y_c2	D_c2	class	distance	az_N
-6.8566	13.401	4.4961	-6.9113	13.435	4.4342	5	3.7331	302.55
-32.518	23.391	3.866	-32.613	23.407	3.0373	6	5.2371	280.32
-0.096961	23.667	20.68	0.21746	23.669	13.471	5	17.036	89.754
40.154	5.5516	7.9578	40.202	5.6028	4.9148	4	4.1301	42.831
33.559	2.317	8.0469	33.473	2.4145	6.5772	6	7.679	318.64
0.66504	9.8942	6.2289	0.66046	9.9404	5.9053	2	2.7461	354.43
43.2	8.9903	5.7868	43.211	8.9265	4.1748	5	3.8234	170.61
61.101	5.881	39.489	61.175	6.4815	33.812	6	35.786	6.956
83.102	1.7725	7.2818	83.071	1.6704	6.4002	5	6.3134	196.95
50.985	20.419	5.6613	50.933	20.469	4.8012	5	4.1214	315.21
88.566	21.284	5.916	88.567	21.32	5.9139	2	2.1287	2.0613
85.302	6.9184	4.7803	85.378	6.9938	4.5353	6	6.3396	45.303
80.309	10.311	4.812	80.32	10.256	3.9909	5	3.3432	169.79
81.01	7.4815	4.3416	81.012	7.4469	2.2234	3	2.0535	176.28
51.971	13.325	3.9889	51.947	13.353	3.0739	5	2.1992	320.6
112.99	13.541	7.8154	113.09	13.539	4.3986	4	5.673	90.994
97.787	28.436	6.533	97.802	28.485	3.2629	3	3.006	14.857
109.79	28.152	6.1552	109.88	28.088	4.108	6	6.2184	127.74
101.36	16.867	5.4931	101.44	16.811	4.9998	6	5.5204	126.56
140.3	28.982	13.509	140.22	29.104	7.7694	4	8.4368	329.03
175.06	14.811	5.1558	175.02	14.848	4.1512	5	3.0915	315.17
139.41	23.087	3.9043	139.45	23.094	2.6916	5	2.2985	79.268
-166.47	-25.893	9.2007	-166.44	-25.99	8.1162	5	6.0483	162.33
-176.35	-15.947	7.476	-176.36	-15.98	4.5111	1	1.9849	189.66
-155.78	-27.476	6.0917	-155.8	-27.489	5.5633	1	1.226	230.21
-158.07	-12.255	5.533	-158.08	-12.224	4.3496	2	1.9115	346.46
-146.79	-28.364	4.0316	-146.77	-28.364	3.7748	1	1.0444	89.882
-159.38	-17.753	3.988	-159.42	-17.761	3.871	5	2.3532	257.86
-165.04	-16.979	3.834	-165.08	-16.972	3.6875	5	1.9637	283.18
-102.37	-1.8666	20.092	-102.57	-1.8939	19.975	5	11.874	262.16
-95.599	-11.605	15.824	-95.663	-11.859	10.504	6	15.481	193.8
-94.538	-16.905	4.5169	-94.563	-16.942	4.1684	5	2.6169	212.93
-76.736	-10.8	10.358	-76.832	-10.865	9.3635	5	6.7788	235.81
-53.036	-17.108	7.2823	-52.96	-17.114	6.749	5	4.3408	95.011
-58.229	-7.7861	6.4911	-58.266	-7.8697	4.8623	5	5.4109	203.92
-75.543	-26.534	5.2407	-75.579	-26.488	2.1928	4	3.2916	325.11
-2.8351	-9.2674	19.45	-2.5121	-9.3152	10.542	6	19.063	98.532
-25.523	-25.88	7.1355	-25.492	-25.943	2.6091	1	4.0687	156.14
-34.638	-21.076	5.9969	-34.664	-21.067	4.4749	1	1.4963	290.14
-10.241	-21.398	5.3745	-10.289	-21.437	3.3104	4	3.5438	229.03
-4.2043	-25.573	4.5088	-4.1803	-25.565	2.5355	3	1.3682	69.898
-44.825	-20.999	4.1919	-44.859	-21.001	1.9309	3	1.8336	266.9
-13.66	-17.873	3.8574	-13.711	-17.896	3.3118	5	3.2043	244.3
35.362	-29.414	19.152	35.187	-29.36	9.2302	4	9.6125	289.43
3.1672	-27.435	15.929	3.4822	-27.25	15.726	6	19.832	56.573
43.298	-17.918	9.5653	43.316	-18.08	5.079	6	9.6225	173.89
0.79477	-17.844	8.8443	0.84292	-17.774	2.4544	1	4.932	33.355
9.4447	-13.005	6.9871	9.4538	-12.965	3.9542	3	2.4333	12.414
2.4474	-20.65	6.5369	2.3975	-20.659	2.8655	3	2.8171	258.59
39.067	-26.906	5.3702	39.111	-26.885	4.407	2	2.6368	60.833
11.342	-5.9463	4.0025	11.29	-5.9464	3.1276	5	3.058	269.8
37.843	-13.723	3.9391	37.837	-13.692	3.6753	2	1.8839	348.53
63.787	-4.2848	8.4488	63.865	-4.2733	5.5692	5	4.6501	81.531
52.463	-25.142	7.566	52.531	-25.109	6.3888	5	4.1412	61.868

Continued on next page

Table2 – continued from previous page

X_c1	Y_c1	D_c1	X_c2	Y_c2	D_c2	class	distance	az_N
67.27	-22.338	8.5262	67.219	-22.326	7.6396	2	2.898	284.74
89.267	-16.009	6.9462	89.266	-15.977	5.6337	1	1.8905	357.6
84.1	-19.914	7.0308	84.078	-19.853	5.8956	5	3.835	341.44
53.066	-2.38	6.7764	53.009	-2.3403	5.6617	5	4.1198	304.81
69.85	-15.319	6.3123	69.825	-15.375	3.566	4	3.6067	203.73
80.78	-2.7819	5.9231	80.721	-2.8369	5.7075	5	4.7508	226.82
48.953	-24.65	4.2747	48.944	-24.631	3.8981	1	1.2478	335.77
75.262	-7.5109	3.9622	75.261	-7.5419	3.7361	2	1.8333	181.84
125.66	-28.479	21.834	125.67	-28.62	11.378	3	8.3769	176.39
110.28	-16.476	11.305	110.31	-16.614	5.0191	4	8.2729	168.76
127.99	-19.314	11.346	127.87	-19.382	3.7839	1	7.6516	238.55
124.65	-24.626	10.004	124.5	-24.684	8.1785	5	8.8319	247.01
124.22	-3.702	7.9665	124.31	-3.6882	4.5907	4	5.8354	81.948
106.63	-22.88	11.345	106.83	-22.813	7.4287	6	11.641	70.201
126.17	-24.587	6.3882	126.26	-24.624	5.5724	5	5.3788	114.1
122.59	-15.589	5.8083	122.55	-15.567	2.0998	1	2.7277	298.29
129.14	-23.935	5.7217	129.18	-23.964	3.5083	3	2.7115	129.73
96.46	-10.296	5.0406	96.57	-10.312	5.016	6	6.4532	98.004
91.46	-7.5541	4.7793	91.449	-7.5015	4.2022	5	3.1785	348.49
101.89	-1.7391	3.7315	101.88	-1.7705	2.0447	4	2.0664	205.96
117.33	-10.417	3.9567	117.35	-10.387	1.8788	3	1.9042	22.668
154.42	-29.58	8.382	154.38	-29.562	4.7057	1	2.3587	296
140.34	-19.204	7.5959	140.33	-19.248	4.1792	3	2.6526	193.11
-174.71	-31.72	6.3251	-174.69	-31.783	3.4732	4	3.8323	167.28
-138.63	-44.502	5.297	-138.6	-44.451	2.1303	4	3.3464	24.251
-160.59	-33.487	4.1318	-160.61	-33.434	4.0483	5	3.3054	341.3
-60.236	-35.458	7.3062	-60.185	-35.371	3.9719	4	5.7302	25.762
-78.247	-30.773	4.4607	-78.213	-30.812	3.907	5	2.8815	143.01
-61.873	-36.826	3.6149	-61.894	-36.806	1.8453	3	1.5226	320.59
-29.097	-33.182	6.6764	-29.138	-33.171	2.8483	3	2.1392	287.39
-19.02	-31.243	6.385	-18.977	-31.244	3.5257	3	2.175	92.142
-13.241	-33.276	5.1755	-13.277	-33.287	2.061	1	1.8605	249.03
-9.346	-36.409	5.3515	-9.3158	-36.431	3.0436	3	1.9358	132.08
-55.268	-39.192	4.7405	-55.317	-39.148	3.0893	5	3.4193	319.03
29.46	-33.244	4.8951	29.401	-33.182	4.5251	6	4.6863	321.8
3.2562	-36.149	4.4731	3.2621	-36.109	1.5803	1	2.3842	6.7516
117.93	-35.603	9.0908	117.75	-35.604	7.8785	6	8.4094	269.87
131.15	-32.633	12.538	131.1	-32.724	8.2709	2	5.8806	203.78
151.42	-47.372	9.5064	151.57	-47.446	8.8219	5	7.2029	127.43
140.2	-30.383	6.8368	140.21	-30.434	3.7132	3	3.0587	171.84
140.48	-36.126	6.6605	140.42	-36.104	4.0193	3	3.2834	292.85
147.99	-35.906	3.6504	148.01	-35.92	2.9758	1	1.0732	136.03

References

Archinal, B.A., Acton, C.H., A'Hearn, M.F., Conrad, A., Consolmagno, G.J., Duxbury, T., Hestroffer, D., Hilton, J.L., Kirk, R.L., Klioner, S.A., McCarthy, D., Meech, K., Oberst, J., Ping, J., Seidelmann, P.K., Tholen, D.J., Thomas, P.C., Williams, I.P., 2018. Report of the IAU Working Group on Cartographic Coordinates and Rotational Elements: 2015. Celestial Mechanics and Dynamical Astronomy 130, 22. doi:10.1007/s10569-017-9805-5.

Baluyev, R.V., Kholshevnikov, K.V., 2005. Distance Between Two Arbitrary Unperturbed Orbits. Celestial Mechanics and Dynamical Astronomy 91, 287–300. doi:10.1007/s10569-004-3207-1.

Bartczak, P., Kryszczyńska, A., Dudziński, G., Polińska, M., Colas, F., Vachier, F., Marciniak, A., Pollock, J., Apostolovska, G., Santana-Ros, T., Hirsch, R., Dimitrow, W., Murawiecka, M., Wietrzycka, P., Nadolny, J., 2017. A new non-convex model of the binary asteroid (809) Lundia obtained with the SAGE modelling technique. MNRAS 471, 941–947. doi:10.1093/mnras/stx1603, arXiv:1905.08336.

Benner, L.A.M., Busch, M.W., Giorgini, J.D., Taylor, P.A., Margot, J.L., 2015. Radar Observations of Near-Earth and Main-Belt Asteroids. pp. 165–182. doi:10.2458/azu_uapress_9780816532131-ch009.

Benner, L.A.M., Nolan, M.C., Margot, J.L., Ostro, S.J., Giorgini, J.D., 2003. Radar Imaging of Binary Near-Earth Asteroid 1998 ST27, in: AAS/Division for Planetary Sciences Meeting Abstracts #35, p. 24.01.

Berthier, J., Vachier, F., Marchis, F., Ďurech, J., Carry, B., 2014. Physical and dynamical properties of the main belt triple Asteroid (87) Sylvia. Icarus 239, 118–130. doi:10.1016/j.icarus.2014.05.046.

Bottke, W.F., Morbidelli, A., Jedicke, R., Petit, J.M., Levison, H.F., Michel, P., Metcalfe, T.S., 2002. Debiased Orbital and Absolute Magnitude Distribution of the Near-Earth Objects. Icarus 156, 399–433. URL: https://ui.adsabs.harvard.edu/abs/2002Icar..156..399B, doi:10.1006/icar.2001.6788.

Bottke, Jr., W.F., Melosh, H.J., 1996. The formation of asteroid satellites and doublet craters by planetary tidal forces. Nature 381, 51–53. doi:10.1038/381051a0.

Bouley, S., Baratoux, D., Matsuyama, I., Forget, F., Séjourné, A., Turbet, M., Costard, F., 2016. Late tharsis formation and implications for early mars. Nature 531, 344–347. doi:https://doi.org/10.1038/nature17171.

Brozović, M., Benner, L.A.M., Taylor, P.A., Nolan, M.C., Howell, E.S., Magri, C., Scheeres, D.J., Giorgini, J.D., Pollock, J.T., Pravec, P., Galád, A., Fang, J., Margot, J.L., Busch, M.W., Shepard, M.K., Reichart, D.E., Ivarsen, K.M., Haislip, J.B., Lacluyze, A.P., Jao, J., Slade, M.A., Lawrence, K.J., Hicks, M.D., 2011. Radar and optical observations and physical modeling of triple near-Earth Asteroid (136617) 1994 CC. Icarus 216, 241–256. doi:10.1016/j.icarus.2011.09.002.

Carry, B., 2012. Density of asteroids. Planet. Space Sci. 73, 98–118. doi:10.1016/j.pss.2012.03.009.

Carry, B., Hestroffer, D., DeMeo, F., Thirouin, A., Berthier, J., Lacerda, P., Sicardy, B., Doressoundiram, A., Dumas, C., Farrelly, D., Müller, T.G., 2011. Integral-field spectroscopy of (90482) Orcus-Vanth. A&A 534, A115. doi:10.1051/0004-6361/201117486.

Carry, B., Matter, A., Scheirich, P., Pravec, P., Molnar, L., Mottola, S., Carbognani, A., Jehin, E., Marciniak, A., Binzel, R.P., DeMeo, F., Birlan, M., Delbo, M., Barbotin, E., Behrend, R., Bonnardeau, M., Colas, F., Farissier, P., Fauvaud, M., Fauvaud, S., Gillier, C., Gillon, M., Hellmich, S., Hirsch, R., Leroy, A., Manfroid, J., Montier, J., Morelle, E., Richard, F., Sobkowiak, K., Strajnic, J., Vachier, F., 2015. The small binary asteroid (939) Isberga. Icarus 248, 516–525. doi:10.1016/j.icarus.2014.11.002.

Chapman, C.R., 2007. Implications for small-body binaries from doublet craters, in: 1st Workshop on Binaries in the Solar System. URL: http://www.boulder.swri.edu/clark/bincra07.ppt.

Chapman, C.R., Veverka, J., Thomas, P.C., Klaasen, K., Belton, M.J.S., Harch, A., McEwen, A., Johnson, T.V., Helfenstein, P., Davies, M.E., Merline, W.J., Denk, T., 1995. Discovery and physical properties of Dactyl, a satellite of asteroid 243 Ida. Nature 374, 783–785. doi:10.1038/374783a0.

Collins, G.S., Melosh, H.J., Marcus, R.A., 2005. Earth impact effects program: A web-based computer program for calculating the regional environmental consequences of a meteoroid impact on earth. Meteoritics & Planetary Science 40, 817–840. URL: https://onlinelibrary.wiley.com/doi/abs/10.1111/j.1945-5100.2005.tb00157.x, doi:https://doi.org/10.1111/j.1945-5100.2005.tb00157.x.

Cook, C.M., Melosh, H.J., Bottke, W.F., 2003. Doublet craters on Venus. Icarus 165, 90–100. doi:10.1016/S0019-1035(03)00177-5.

Dickson, J.L., Kerber, L., Fassett, C.I., Ehlmann, B.L., 2018. A global, blended CTX mosaic of Mars with vectorized seam mapping: a new mosaicking pipeline using principles of non-destructive image editing, in: 49th Lunar and Planetary Science Conference.

Drummond, J.D., Merline, W.J., Carry, B., Conrad, A., Tamblyn, P., Enke, B., Christou, J., Dumas, C., Chapman, C.R., Durda, D.D., Owen, W.M., Grundy, W.M., Reynolds, O.R., Buckman, M.D., 2021. The orbit of asteroid (317) Roxane's satellite Olympias from Gemini, Keck, VLT and the SOR, and (22) Kalliope's Linus from the SOR. Icarus 358, 114275. doi:10.1016/j.icarus.2020.114275.

Dunham, D.W., Herald, D., Frappa, E., Hayamizu, T., Talbot, J., Timerson, B., 2017. Asteroid Occultations. NASA Planetary Data System. EAR-A-3-RDR-OCCULTATIONS-V15.0.

Durda, D.D., Bottke, W.F., Enke, B.L., Merline, W.J., Asphaug, E., Richardson, D.C., Leinhardt, Z.M., 2004. The formation of asteroid satellites in large impacts: results from numerical simulations. Icarus 170, 243–257. doi:10.1016/j.icarus.2004.04.003.

Edwards, C.S., Nowicki, K.J., Christensen, P.R., Hill, J., Gorelick, N., Murray, K., 2011. Mosaicking of global planetary image datasets: 1. Techniques and data processing for Thermal Emission Imaging System (THEMIS) multi-spectral data. Journal of Geophysical Research 116, E10008. doi:10.1029/2010JE003755.

Elbeshausen, D., Wünnemann, K., Collins, G.S., 2013. The transition from circular to elliptical impact craters. Journal of Geophysical Research: Planets 118, 2295–2309. doi:10.1002/2013JE004477.

Everhart, E., 1985. An efficient integrator that uses Gauss-Radau spacings. volume 115. p. 185. doi:10.1007/978-94-009-5400-7_17.

Fang, J., Margot, J.L., 2012. Near-Earth Binaries and Triples: Origin and Evolution of Spin-Orbital Properties. AJ 143, 24. doi:10.1088/0004-6256/143/1/24, arXiv:1111.2794.

Ferreira, J.F., Tanga, P., Machado, P., Corsaro, E., 2020. A survey for occultation astrometry of main belt: expected astrometric performances. A&A 641, A81. doi:10.1051/0004-6361/202038190, arXiv:2007.09665.

Fevig, R.A., Wren, P.F., 2019. Comparing binary systems of the inner and intermediate zones of the asteroid belt, in: 10th Meeting of the Planetary Crater Consortium, Unpublished. doi:10.13140/RG.2.2.27144.37125.

Fujiwara, A., Kawaguchi, J., Yeomans, D.K., Abe, M., Mukai, T., Okada, T., Saito, J., Yano, H., Yoshikawa, M., Scheeres, D.J., Barnouin-Jha, O.S., Cheng, A.F., Demura, H., Gaskell, G.W., Hirata, N., Ikeda, H., Kominato, T., Miyamoto, H., Nakamura, R., Sasaki, S., Uesugi, K., 2006. The Rubble-Pile Asteroid Itokawa as Observed by Hayabusa. Science 312, 1330–1334.

Gault, D.E., Wedekind, J.A., 1978. Experimental studies of oblique impact, in: New York, Pergamon Press, I. (Ed.), Lunar and Planetary Science Conference, 9th, Houston, Tex., March 13-17, Proceedings., pp. 3843–3875.

Granvik, M., Morbidelli, A., Vokrouhlický, D., Bottke, W.F., Nesvorný, D., Jedicke, R., 2017. Escape of asteroids from the main belt. A&A 598, A52. doi:10.1051/0004-6361/201629252.

Hanuš, J., Ďurech, J., Brož, M., Marciniak, A., Warner, B.D., Pilcher, F., Stephens, R., Behrend, R., Carry, B., Čapek, D., Antonini, P., Audejean, M., Augustesen, K., Barbotin, E., Baudouin, P., Bayol, A., Bernasconi, L., Borczyk, W., Bosch, J.G., Brochard, E., Brunetto, L., Casulli, S., Cazenave, A., Charbonnel, S., Christophe, B., Colas, F., Coloma, J., Conjat, M., Cooney, W., Correira, H., Cotrez, V., Coupier, A., Crippa, R., Cristofanelli, M., Dalmas, C., Danavaro, C., Demeautis, C., Droege, T., Durkee, R., Esseiva, N., Esteban, M., Fagas, M., Farroni, G., Fauvaud, M., Fauvaud, S., Del Freo, F., Garcia, L., Geier, S., Godon, C., Grangeon, K., Hamanowa, H., Hamanowa, H., Heck, N., Hellmich, S., Higgins, D., Hirsch, R., Husarik, M., Itkonen, T., Jade, O., Kamiński, K., Kankiewicz, P., Klotz, A., Koff, R.A., Kryszczyńska, A., Kwiatkowski, T., Laffont, A., Leroy, A., Lecacheux, J., Leonie, Y., Leyrat, C., Manzini,

F., Martin, A., Masi, G., Matter, D., Michałowski, J., Michałowski, M.J., Michałowski, T., Michelet, J., Michelsen, R., Morelle, E., Mottola, S., Naves, R., Nomen, J., Oey, J., Ogłoza, W., Oksanen, A., Oszkiewicz, D., Pääkkönen, P., Paiella, M., Pallares, H., Paulo, J., Pavic, M., Payet, B., Polińska, M., Polishook, D., Poncy, R., Revaz, Y., Rinner, C., Rocca, M., Roche, A., Romeuf, D., Roy, R., Saguin, H., Salom, P.A., Sanchez, S., Santacana, G., Santana-Ros, T., Sareyan, J.P., Sobkowiak, K., Sposetti, S., Starkey, D., Stoss, R., Strajnic, J., Teng, J.P., Trégon, B., Vagnozzi, A., Velichko, F.P., Waelchli, N., Wagrez, K., Wücher, H., 2013. Asteroids' physical models from combined dense and sparse photometry and scaling of the YORP effect by the observed obliquity distribution. A&A 551, A67. doi:10.1051/0004-6361/201220701.

Harris, A.W., Warner, B.D., Pravec, P., 2017. Asteroid Lightcurve Derived Data V17.0. NASA Planetary Data System .

Holo, S.J., Kite, E.S., Robbins, S.J., 2018. Mars obliquity history constrained by elliptic crater orientations. Earth and Planetary Science Letters 496, 206–214. URL: https://www.sciencedirect.com/science/article/pii/S0012821X18303297, doi:https://doi.org/10.1016/j.epsl.2018.05.046.

Jacobson, S.A., Scheeres, D.J., 2011. Dynamics of rotationally fissioned asteroids: Source of observed small asteroid systems. Icarus 214, 161–178. doi:10.1016/j.icarus.2011.04.009, arXiv:1404.0801.

Jacobson, S.A., Scheeres, D.J., McMahon, J., 2014. Formation of the Wide Asynchronous Binary Asteroid Population. ApJ 780, 60. doi:10.1088/0004-637X/780/1/60, arXiv:1311.4887.

Johnston, W.R., 2018. Binary Minor Planets Compilation V2.0. NASA Planetary Data System .

Jourdan, F., Reimold, W.U., Deutsch, A., 2012. Dating Terrestrial Impact Structures. Elements 8, 49–53. URL: https://doi.org/10.2113/gselements.8.1.49, doi:10.2113/gselements.8.1.49, arXiv:https://pubs.geoscienceworld.org/elements/article-pdf/8/1/49/3166168/gselements.8.1.49.pdf.

Kite, E.S., Matsuyama, I., Manga, M., Perron, J.T., Mitrovica, J.X., 2009. True polar wander driven by late-stage volcanism and the distribution of paleopolar deposits on mars. Earth and Planetary Science Letters 280, 254–267. URL: https://www.sciencedirect.com/science/article/pii/S0012821X09000739, doi:https://doi.org/10.1016/j.epsl.2009.01.040.

Kizner, W., 1961. A Method of Describing Miss Distances for Lunar and Interplanetary Trajectories. Planet. Space Sci. 7, 125–131. doi:10.1016/0032-0633(61)90293-8.

Kneissl, T., van Gasselt, S., Neukum, G., 2011. Map-projection-independent crater size-frequency determination in gis environments—new software tool for arcgis. Planetary and Space Science 59, 1243–1254. URL: https://www.sciencedirect.com/science/article/pii/S0032063310000887, doi:https://doi.org/10.1016/j.pss.2010.03.015. geological Mapping of Mars.

Komatsu, G., Ori, G.G., Di Lorenzo, S., Rossi, A.P., Neukum, G., 2007. Combinations of processes responsible for martian impact crater "layered ejecta structures" emplacement. Journal of Geophysical Research: Planets 112. URL: https://agupubs.onlinelibrary.wiley.com/doi/abs/10.1029/2006JE002787, doi:https://doi.org/10.1029/2006JE002787, arXiv:https://agupubs.onlinelibrary.wiley.com/doi/pdf/10.1029/2006JE002787.

La Spina, A., Paolicchi, P., Kryszczyńska, A., Pravec, P., 2004. Retrograde spins of near-Earth asteroids from the Yarkovsky effect. Nature 428, 400–401. doi:10.1038/nature02411.

Lagain, A., Bouley, S., Baratoux, D., Costard, F., Wieczorek, M., 2020. Impact cratering rate consistency test from ages of layered ejecta on Mars. Planetary and Space Science 180, 104755. URL: https://www.sciencedirect.com/science/article/pii/S0032063319301904, doi:https://doi.org/10.1016/j.pss.2019.104755.

Lagain, A., Bouley, S., Baratoux, D., Marmo, C., Costard, F., Delaa, O., Pio Rossi, A., Minin, M., Benedix, G.K., Ciocco, M., Bedos, B., Guimpier, A., Dehouck, E., Loizeau, D., Bouquety, A., Zhao, J., Vialatte, A., Cormau, M., Le Conte des Floris, E., Schmidt, F., Thollot, P., Champion, J., Martinot, M., Gargani, J., Beck, P., Boisson, J., Paulien, N., Séjourné, A., Pasquon, K., Christoff, N., Belgacem, I., Landais, F., Rousseau, B., Dupeyrat, L., Franco, M., Andrieu, F., Cecconi, B., Erard, S., Jabaud, B., Malarewicz, V., Beggiato, G., Janez, G., Elbaz, L., Ourliac, C., Catheline, M., Fries, M., Karamoko, A., Rodier, J., Sarian, R., Gillet, A., Girard, S., Pottier, M., Strauss, S., Chanon, C., Lavaud, P., Boutaric, A., Savourat, M., Garret, E., Leroy, E., Geffray, M.C., Parquet, L., Delagoutte, M.A., Gamblin, O., 2021. Crater database: A participative project for the classification of Martian craters´ morphological characteristics, in: Large Meteorite Impacts and Planetary Evolution VI. Geological Society of America. chapter Structural geology and morphometry of impact structures – on Earth and Mars. doi:10.1130/2021.2550(29).

Lagain, A., Guimpier, A., Bouley, S., 2017. Martian double craters recognition by dating method, in: 48th Lunar and Planetary Science Conference.

Laskar, J., Correia, A.C.M., Gastineau, M., Joutel, F., Levrard, B., Robutel, P., 2004. Long term evolution and chaotic diffusion of the insolation quantities of Mars. Icarus 170, 343–364. doi:10.1016/j.icarus.2004.04.005.

Marchis, F., Kaasalainen, M., Hom, E.F.Y., Berthier, J., Enriquez, J., Hestroffer, D., Le Mignant, D., de Pater, I., 2006. Shape, size and multiplicity of main-belt asteroids. Icarus 185, 39–63. URL: https://ui.adsabs.harvard.edu/abs/2006Icar..185...39M, doi:10.1016/j.icarus.2006.06.001.

Margot, J.L., Brown, M.E., 2003. A Low-Density M-type Asteroid in the Main Belt. Science 300, 1939–1942. doi:10.1126/science.1085844.

Margot, J.L., Nolan, M.C., Benner, L.A.M., Ostro, S.J., Jurgens, R.F., Giorgini, J.D., Slade, M.A., Campbell, D.B., 2002. Binary Asteroids in the Near-Earth Object Population. Science 296, 1445–1448. doi:10.1126/science.1072094.

Margot, J.L., Pravec, P., Taylor, P., Carry, B., Jacobson, S., 2015. Asteroid Systems: Binaries, Triples, and Pairs. Univ. Arizona Press. pp. 355–374. doi:10.2458/azu_uapress_9780816532131-ch019.

Marsden, B.G., 1993. To hit or not to hit, in: Canavan, G.H., Solem, J.C., Rather, J.D.G. (Eds.), Proceedings of the Near-Earth-Objects Interception Workshop, pp. 67–71.

Marsset, M., Brož, M., Vernazza, P., Drouard, A., Castillo-Rogez, J., Hanuš, J., Viikinkoski, M., Rambaux, N., Carry, B., Jorda, L., Ševeček, P., Birlan, M., Marchis, F., Podlewska-Gaca, E., Asphaug, E., Bartczak, P., Berthier, J., Cipriani, F., Colas, F., Dudziński, G., Dumas, C., Durech, J., Ferrais, M., Fétick, R., Fusco, T., Jehin, E., Kaasalainen, M., Kryszczynska, A., Lamy, P., Le Coroller, H., Marciniak, A., Michalowski, T., Michel, P., Richardson, D.C., Santana-Ros, T., Tanga, P., Vachier, F., Vigan, A., Witasse, O., Yang, B., 2020. The violent collisional history of aqueously evolved (2) Pallas. Nature Astronomy 4, 569–576. doi:10.1038/s41550-019-1007-5.

Melosh, H.J., Ingram, J., Bottke, W.F., 1996. The Abundance of Doublet Craters on Mars, in: Lunar and Planetary Science Conference, p. 863.

Melosh, H.J., Stansberry, J.A., 1991. Doublet craters and the tidal disruption of binary asteroids. Icarus 94, 171–179. doi:10.1016/0019-1035(91)90148-M.

Merline, W.J., Close, L.M., Dumas, C., Chapman, C.R., Roddier, F., Ménard, F., Slater, D.C., Duvert, G., Shelton, C., Morgan, T., 1999. Discovery of a moon orbiting the asteroid 45 Eugenia. Nature 401, 565–568.

Merline, W.J., Weidenschilling, S.J., Durda, D.D., Margot, J.L., Pravec, P., Storrs, A.D., 2002. Asteroids Do Have Satellites. Asteroids III , 289–312.

Miljković, K., Collins, G.S., Mannick, S., Bland, P.A., 2013. Morphology and population of binary asteroid impact craters. Earth and Planetary Science Letters 363, 121–132. doi:10.1016/j.epsl.2012.12.033.

Oberbeck, V.R., 1973. Simultaneous impact and lunar craters. The Moon 6, 83–92. doi:10.1007/BF02630653.

Oberbeck, V.R., 1975. The role of ballistic erosion and sedimentation in lunar stratigraphy. Reviews of Geophysics 13, 337–362. URL: https://agupubs.onlinelibrary.wiley.com/doi/abs/10.1029/RG013i002p00337, doi:https://doi.org/10.1029/RG013i002p00337, arXiv:https://agupubs.onlinelibrary.wiley.com/doi/pdf/10.1029/RG013i002p00337.

Ormö, J., Sturkell, E., Nõlvak, J., Melero-Asensio, I., Frisk, A., Wikström, T., 2014. The geology of the målingen structure: A probable doublet to the lockne marine-target impact crater, central sweden. Meteoritics & Planetary Science 49, 313–327. URL: https://onlinelibrary.wiley.com/doi/abs/10.1111/maps.12251, doi:https://doi.org/10.1111/maps.12251,

arXiv:https://onlinelibrary.wiley.com/doi/pdf/10.1111/maps.12251.

Ostro, S.J., Benner, L.A.M., Magri, C., Giorgini, J.D., Rose, R., Jurgens, R.F., Yeomans, D.K., Hine, A.A., Nolan, M.C., Scheeres, D.J., Broschart, S.B., Kaasalainen, M., Margot, J.L., 2005. Radar observations of Itokawa in 2004 and improved shape estimation. Meteoritics and Planetary Science 40, 1563–1574. doi:10.1111/j.1945-5100.2005.tb00131.x.

Ostro, S.J., Magri, C., Benner, L.A.M., Giorgini, J.D., Nolan, M.C., Hine, A.A., Busch, M.W., Margot, J.L., 2010. Radar imaging of Asteroid 7 Iris. Icarus 207, 285–294. doi:10.1016/j.icarus.2009.11.011.

Pajuelo, M., Carry, B., Vachier, F., Marsset, M., Berthier, J., Descamps, P., Merline, W.J., Tamblyn, P.M., Grice, J., Conrad, A., Storrs, A., Timerson, B., Dunham, D., Preston, S., Vigan, A., Yang, B., Vernazza, P., Fauvaud, S., Bernasconi, L., Romeuf, D., Behrend, R., Dumas, C., Drummond, J.D., Margot, J.L., Kervella, P., Marchis, F., Girard, J.H., 2018. Physical, spectral, and dynamical properties of asteroid (107) Camilla and its satellites. Icarus 309, 134–161. doi:10.1016/j.icarus.2018.03.003, arXiv:1803.02722.

Perets, H.B., Naoz, S., 2009. Kozai Cycles, Tidal Friction, and the Dynamical Evolution of Binary Minor Planets. ApJ 699, L17–L21. doi:10.1088/0004-637X/699/1/L17, arXiv:0809.2095.

Polishook, D., Brosch, N., Prialnik, D., 2011. Rotation periods of binary asteroids with large separations - Confronting the Escaping Ejecta Binaries model with observations. Icarus 212, 167–174. doi:10.1016/j.icarus.2010.12.020, arXiv:1012.4810.

Pravec, P., Harris, A.W., 2007. Binary asteroid population. 1. Angular momentum content. Icarus 190, 250–259. doi:10.1016/j.icarus.2007.02.023.

Pravec, P., Scheirich, P., Kušnirák, P., Šarounová, L., Mottola, S., Hahn, G., Brown, P.G., Esquerdo, G.A., Kaiser, N., Krzeminski, Z., Pray, D.P., Warner, B.D., Harris, A.W., Nolan, M.C., Howell, E.S., Benner, L.A.M., Margot, J.L., Galád, A., Holliday, W., Hicks, M.D., Krugly, Y.N., Tholen, D.J., Whiteley, R.J., Marchis, F., Degraff, D.R., Grauer, A., Larson, S., Velichko, F.P., Cooney, W.R., Stephens, R., Zhu, J., Kirsch, K., Dyvig, R., Snyder, L., Reddy, V., Moore, S., Gajdoš, Š., Világi, J., Masi, G., Higgins, D., Funkhouser, G., Knight, B., Slivan, S.M., Behrend, R., Grenon, M., Burki, G., Roy, R., Demeautis, C., Matter, D., Waelchli, N., Revaz, Y., Klotz, A., Rieugné, M., Thierry, P., Cotrez, V., Brunetto, L., Kober, G., 2006. Photometric survey of binary near-Earth asteroids. Icarus 181, 63–93. doi:10.1016/j.icarus.2005.10.014.

Pravec, P., Scheirich, P., Vokrouhlický, D., Harris, A.W., Kušnirák, P., Hornoch, K., Pray, D.P., Higgins, D., Galád, A., Világi, J., Gajdoš, Š., Kornoš, L., Oey, J., Husárik, M., Cooney, W.R., Gross, J., Terrell, D., Durkee, R., Pollock, J., Reichart, D.E., Ivarsen, K., Haislip, J., Lacluyze, A., Krugly, Y.N., Gaftonyuk, N., Stephens, R.D., Dyvig, R., Reddy, V., Chiorny, V., Vaduvescu, O., Longa-Peña, P., Tudorica, A., Warner, B.D., Masi, G., Brinsfield, J., Gonçalves, R., Brown, P., Krzeminski, Z., Gerashchenko, O., Shevchenko, V., Molotov, I., Marchis, F., 2012. Binary asteroid population. 2. Anisotropic distribution of orbit poles of small, inner main-belt binaries. Icarus 218, 125–143. doi:10.1016/j.icarus.2011.11.026.

Pravec, P., Vokrouhlický, D., Polishook, D., Scheeres, D.J., Harris, A.W., Galád, A., Vaduvescu, O., Pozo, F., Barr, A., Longa, P., Vachier, F., Colas, F., Pray, D.P., Pollock, J., Reichart, D., Ivarsen, K., Haislip, J., Lacluyze, A., Kušnirák, P., Henych, T., Marchis, F., Macomber, B., Jacobson, S.A., Krugly, Y.N., Sergeev, A.V., Leroy, A., 2010. Formation of asteroid pairs by rotational fission. Nature 466, 1085–1088. doi:10.1038/nature09315.

Pravec, P., Wolf, M., Sarounova, L., 1997. 1991 vh. IAU Circular 6607.

Robbins, S.J., Hynek, B.M., 2012a. A new global database of Mars impact craters ≥1 km: 1. Database creation, properties, and parameters. Journal of Geophysical Research (Planets) 117, E05004. doi:10.1029/2011JE003966.

Robbins, S.J., Hynek, B.M., 2012b. A new global database of Mars impact craters ≥1 km: 2. Global crater properties and regional variations of the simple-to-complex transition diameter. Journal of Geophysical Research (Planets) 117, E06001. doi:10.1029/2011JE003967.

Robbins, S.J., Hynek, B.M., 2012. A new global database of mars impact craters 1 km: 2. global crater properties and regional variations of the simple-to-complex transition diameter. Journal of Geophysical Research: Planets 117. URL: https://agupubs.onlinelibrary.wiley.com/doi/abs/10.1029/2011JE003967, doi:https://doi.org/10.1029/2011JE003967, arXiv:https://agupubs.onlinelibrary.wiley.com/doi/pdf/10.1029/2011JE003967.

Schmieder, M., Kring, D.A., 2020. Earth's impact events through geologic time: A list of recommended ages for terrestrial impact structures and deposits. Astrobiology 20, 91–141. URL: https://doi.org/10.1089/ast.2019.2085, doi:10.1089/ast.2019.2085, arXiv:https://doi.org/10.1089/ast.2019.2085. pMID: 31880475.

Schmieder, M., Trieloff, M., Schwarz, W.H., Buchner, E., Jourdan, F., 2014. Supportive comment on: "morphology and population of binary asteroid impact craters", by k. miljković, g.s. collins, s. mannick and p.a. bland [earth planet. sci. lett. 363 (2013) 121–132] – an updated assessment. Earth and Planetary Science Letters 405, 281–284. URL: https://www.sciencedirect.com/science/article/pii/S0012821X13004913, doi:https://doi.org/10.1016/j.epsl.2013.08.047.

Shepard, M.K., Margot, J.L., Magri, C., Nolan, M.C., Schlieder, J., Estes, B., Bus, S.J., Volquardsen, E.L., Rivkin, A.S., Benner, L.A.M., Giorgini, J.D., Ostro, S.J., Busch, M.W., 2006. Radar and infrared observations of binary near-Earth Asteroid 2002 CE26. Icarus 184, 198–210. doi:10.1016/j.icarus.2006.04.019.

Shepard, M.K., Timerson, B., Scheeres, D.J., Benner, L.A.M., Giorgini, J.D., Howell, E.S., Magri, C., Nolan, M.C., Springmann, A., Taylor, P.A., Virkki, A., 2018. A revised shape model of asteroid (216) Kleopatra. Icarus 311, 197–209. URL: https://ui.adsabs.harvard.edu/#abs/2018Icar..311..197S/abstract, doi:10.1016/j.icarus.2018.04.002.

Storrs, A.D., Dunne, C., Conan, J.M., Mugnier, L.M., Weiss, B.P., Zellner, B.H., 2005. A closer look at main belt asteroids 1: WF/PC images. Icarus 173, 409–416. URL: https://ui.adsabs.harvard.edu/abs/2005Icar..173..409S.

Storrs, A.D., Weiss, B., Zellner, B., Burleson, W., Sichitiu, R., Wells, E., Kowal, C., Tholen, D., 1999. Imaging Observations of Asteroids with Hubble Space Telescope. Icarus 137, 260–268. doi:10.1006/icar.1999.6047.

Tanga, P., Delbo, M., 2007. Asteroid occultations today and tomorrow: toward the GAIA era. A&A 474, 1015–1022. doi:10.1051/0004-6361:20077470.

Thomas, P.C., Binzel, R.P., Gaffey, M.J., Storrs, A.D., Wells, E.N., Zellner, B.H., 1997. Impact excavation on asteroid 4 Vesta: Hubble Space Telescope results. Science 277, 1492–1495.

Thomas, P.C., Parker, J.W., McFadden, L.A., Russell, C.T., Stern, S.A., Sykes, M.V., Young, E.F., 2005. Differentiation of the asteroid Ceres as revealed by its shape. Nature 437, 224–226. doi:10.1038/nature03938.

Timerson, B., Brooks, J., Conard, S., Dunham, D.W., Herald, D., Tolea, A., Marchis, F., 2013. Occultation evidence for a satellite of the Trojan asteroid (911) Agamemnon. Planet. Space Sci. 87, 78–84. doi:10.1016/j.pss.2013.08.015.

Vokrouhlický, D., Bottke, W.F., Chesley, S.R., Scheeres, D.J., Statler, T.S., 2015. The Yarkovsky and YORP Effects. pp. 509–531. URL: https://ui.adsabs.harvard.edu/abs/2015aste.book..509V, doi:10.2458/azu_uapress_9780816532131-ch027.

Walsh, K.J., Jacobson, S.A., 2015. Formation and Evolution of Binary Asteroids. pp. 375–393. doi:10.2458/azu_uapress_9780816532131-ch020.

Walsh, K.J., Richardson, D.C., Michel, P., 2008. Rotational breakup as the origin of small binary asteroids. Nature 454, 188–191. doi:10.1038/nature07078.

Warner, B.D., 2016. Three Additional Candidates for the Group of Very Wide Binary Asteroids. Minor Planet Bulletin 43, 306–309.

Warner, B.D., Stephens, R.D., 2019. Another Trio of Possible Very Wide Binaries. Minor Planet Bulletin 46, 153–157.

Warner, B.D., Stephens, R.D., Harris, A.W., 2018. The Continuing Conundrum of the Very Wide Binary Asteroids, in: AAS/Division for Planetary Sciences Meeting Abstracts #50, p. 417.02.

Weidenschilling, S.J., Paolicchi, P., Zappala, V., 1989. Do asteroids have satellites? Asteroids II , 643–658.

Wren, P.F., Fevig, R.A., 2020. Examining Doublet Craters on the Lunar

Maria to Constrain Binary Asteroids in the Near-Earth Population, in: 11th Planetary Crater Consortium, p. 2061.

Yu, Y., Richardson, D.C., Michel, P., Schwartz, S.R., Ballouz, R.L., 2014. Numerical predictions of surface effects during the 2029 close approach of Asteroid 99942 Apophis. Icarus 242, 82–96. doi:10.1016/j.icarus.2014.07.027.